Ann. Geophys., 43, 621–631, 2025 https://doi.org/10.5194/angeo-43-621-2025 © Author(s) 2025. This work is distributed under the Creative Commons Attribution 4.0 License.





Effects of geomagnetic mirror force and pitch angles of precipitating electrons on ionization of the polar upper atmosphere

Tomotaka M. Tanaka^{1,2}, Yasunobu Ogawa^{1,2}, Yuto Katoh³, Mizuki Fukizawa², Anton Artemyev⁴, Vassilis Angelopoulos⁴, Xiao-Jia Zhang⁵, Yoshimasa Tanaka^{1,2,6}, and Akira Kadokura^{2,6}

Correspondence: Tomotaka M. Tanaka (tanaka.tomotaka@nipr.ac.jp)

Received: 6 March 2025 – Discussion started: 28 March 2025

Revised: 4 August 2025 – Accepted: 8 September 2025 – Published: 20 October 2025

Abstract. We studied the effects of the geomagnetic mirror force on electron density enhancements in the polar atmosphere due to energetic electron precipitation. Using the pitch angle and energy distribution of electrons observed by the low-altitude Electron Losses and Fields INvestigation (ELFIN) satellites as initial conditions, the electron density in the atmosphere caused by precipitating electrons was calculated using a simulation with two different methods: a traditional method that does not include the effect of the mirror force and a recently developed method that includes the effect. From a simultaneous observation event of the ELFIN satellite and the European Incoherent SCATter scientific radar system (EISCAT) Tromsø radar, it was found that the method with the effect of the mirror force reduces electron density by about 40 % at an altitude of 80 km compared to the traditional method. This decrease was pronounced when the pitch angle distribution of high-energy electrons was concentrated in the pitch angle range of the trapped component and near the loss cone. The maximum decrease was 50 %. For an event where the altitude profile of electron density was accurately determined from the EISCAT radar, the electron density profile estimated using the method with the effect of mirror force showed better agreement with the electron density profile derived from the EISCAT radar. The comparison between simulation results and the observation data contributes to the establishment and improvement of atmospheric ionization models using various types of precipitating electrons.

1 Introduction

The energetic (> 50 keV) electron precipitation (EEP) has attracted attention due to its impact on mesospheric ionization and ozone chemistry. Miyoshi et al. (2020) suggested that precipitating energetic electrons penetrate to lower altitudes with the appearance of diffuse auroras. Oyama et al. (2017) reported electron density enhancements in the lower D region ionosphere during pulsating auroral events, attributed to EEP. These enhancements may accelerate chemical reactions and the production of nitrogen or hydrogen oxides, which destroy ozone in the mesosphere below 80 km altitude (Turunen et al., 2016). Thus, it has been suggested that EEP has ability to make chemical changes in the lower altitude based on both observations and simulation (Miyoshi et al., 2021; Ozaki et al., 2022; Murase et al. 2022). However, modeled ionization rates due to EEP can differ by up to an order (Nesse et al., 2021). Therefore, it is necessary to evaluate the effects of EEP on the atmosphere accurately by considering simulation improvements.

The mirror force, one of the effects of the magnetic field on charged particles, has recently been considered in numerical simulations of atmospheric ionization by precipitating elec-

¹Department of Polar Science, The Graduate University for Advanced Studies, SOKENDAI, Tachikawa, Japan

²National Institute of Polar Research, NIPR, Tachikawa, Japan

³Department of Geophysics, Graduate School of Science, Tohoku University, Sendai, Japan

⁴Department of Earth, Planetary, and Space Sciences, University of California, Los Angeles, UCLA, United States of America

⁵Department of Physics, University of Texas, Dallas, UTD, United States of America

⁶Joint Support-Center for Data Science Research, ROIS, Tachikawa, Japan

trons. As the magnetic field strength at atmospheric altitudes is nearly constant, the change in the pitch angle of precipitating electrons by the effect of the mirror force has been considered negligible (Rees, 1963). Even if some numerical simulations included the pitch angle, it was only used to calculate the altitude change of the electron motion using the inclination of the magnetic field and pitch angle. Thus, velocity changes due to the mirror force were still ignored (Solomon, 1993, 2001). A numerical simulation to calculate the altitude profile of atmospheric ionization rate by EEP, including the effect of the mirror force, was developed (Lehtinen et al., 1999), and the results of the simulation were parameterized by the pitch angle and energy of the electron (Xu et al., 2020). Furthermore, using a newly developed simulation, Katoh et al. (2023) showed the concrete difference in ionization rates between cases with and without the effect of the mirror force. By comparing the simulation results with and without the effect, it was found that when an electron with a large pitch angle had energies above 100 keV, the ionization rate of the former was less than 10% of the latter (Katoh et al., 2023). However, this effect has not yet been verified or confirmed by any observational data.

Although some satellites have observed electrons' energy and pitch angle distribution, it has been challenging to use them in simulation as input. The Arase satellite, for example, is too far away to observe the pitch angle distribution of electrons reaching the earth's atmosphere in detail, while the energy range of electrons observed by the Reimei satellite was too low to make differences between cases with and without the effect of the mirror force, as shown in Katoh et al. (2023). However, the ELFIN (Electron Losses and Fields INvestigation CubeSats) satellites, polar-orbiting and low-altitude satellites, observed both pitch angle and energy distribution of energetic electrons. Therefore, it has been possible to evaluate the actual atmospheric effects by combining the satellites with the simulations developed by Katoh et al. (2023).

This study aims to evaluate the effect of the mirror force on atmospheric electron density integrating satellite observations with simulation results and subsequently validating the results with radar data. Even though it is challenging to evaluate the ionization rate, calculating the electron density from the ionization rate enabled us to compare it with observational data. Using the pitch angle and energy distributions of electrons observed by the ELFIN satellites, we calculated the electron density enhancement due to the precipitating electrons with and without the effect separately to compare them with the actual data observed by the EISCAT (European Incoherent Scatter) Tromsø radar. In this study we mainly show comparison results with simulations focusing on the event of 16 December 2021, when the altitude profile of electron density was obtained accurately from EISCAT observations.

2 Methods and Instruments

2.1 ELFIN satellites

We used data from the ELFIN satellites. The satellites were launched in September 2018 and completed observations in September 2022. They were on a low-altitude ($\sim 450 \, \mathrm{km}$ altitude) polar orbit ($\sim 93^{\circ}$ inclination), and the orbital period is about 90 min. It consists of two CubeSats (ELFIN-A/B), flying in nearly identical orbits with a time difference of less than 20 min (Angelopoulos et al., 2020). Each satellite had an energetic particle detector for electrons (EPDE), which measured 50–7000 keV electrons with $\Delta E/E < 40\%$ energy resolution and 22.5° pitch angle resolution. Since the electron flux above 2500 keV is negligible compared to electrons with energies below that, we used the electron flux data between 50 and 2500 keV in this study. The spin axis is kept perpendicular to the orbital plane, and the whole pitch angle is observed twice every spin period ($\sim 2.85 \, \mathrm{s}$) (Zhang et al., 2022). A loss cone angle $\theta_{L.A.}$ is defined as a equation

$$\theta_{\text{L.A.}} = \sin^{-1} \sqrt{\frac{B}{B_{100}}} \tag{1}$$

where B, and B_{100} are the magnetic field strength at the satellite location and at $100 \,\mathrm{km}$ altitude, respectively. In other words, it is the maximum pitch angle of electrons at the satellite point which can enter the atmosphere below $100 \,\mathrm{km}$ altitude while moving in the magnetic field. The IGRF model (Alken et al., 2021) was used as a magnetic field model to calculate the loss cone angle.

2.2 EISCAT Tromsø radar

We also used the EISCAT Tromsø UHF radar, which has been in operation since 1981 at Tromsø (69.6° N, 19.2° E, and magnetic latitude of 66.2°) in northern Scandinavia. This radar observes the altitude profile of electron density and other ionospheric parameters (Folkestad et al., 1983). For all events in this study, the beata pulse code was utilized, and the beam was directed along to the magnetic field line. The electron density data used in this study were obtained with the beam aligned along the magnetic field lines, and were derived from the power profile data using the standard analysis software GUISDAP (Lehtinen and Huuskonen, 1996). Appropriate power calibration was performed by comparing the radar-derived electron densities with the co-located ionosonde measurements (foF2 and foE), and calibration factors were applied accordingly.

2.3 Simulation

The simulation used in this study is a Monte Carlo simulation developed by Katoh et al. (2023). It has atmospheric data of oxygen atoms, oxygen molecules, and nitrogen molecules using the NRLMSIS 2.1 emprical mode (Lucas, 2022; Em-

mert et al., 2022). It enables us to calculate the altitude profile of the ionization rate above Tromsø (L=6.45), using precipitating electron parameters – altitude, pitch angle, and energy – as initial conditions. The effect of the Lorentz force can be included or excluded manually when calculating particle transport. When considering the force, the magnetic field at a distance of Larmor radius from the magnetic field line leading to Tromsø was given to satisfy $\nabla \cdot \mathbf{B} = 0$ and used in the calculations (see Katoh et al., 2023).

2.4 Combination of the ELFIN satellites data and the simulation

First, we searched for events in which either of the ELFIN satellites approached the EISCAT Tromsø radar. We used the IGRF model to calculate the geomagnetic footprints of the satellite, and selected events in which the geomagnetic latitude was within $69.6^{\circ} \text{N} \pm 2^{\circ}$, and the longitude was within $19.2^{\circ} E \pm 5^{\circ}$. Second, we selected events that showed some electron density peak under 100 km altitude or had a density of more than 10^{10} m⁻³ at 85 km altitude in the EISCAT data, which should be caused by the EEP. Next, we used the differential number flux of electrons in each energy and pitch angle bin observed by the satellite as the initial condition of the simulations. For each bin, we simulated the altitude profile of collision rate R [m⁻¹], defined as the number of ionization events produced by a single precipitating electron in each 1 m altitude interval in the atmosphere. For some specific bins containing the loss cone angle, the collision rate was calculated more precisely by dividing the pitch angle range of the bin into ten parts and averaging the results. Katoh et al. (2023) described the method for calculating the collision rate and demonstrated that it varies sensitively with pitch angle near the loss cone angle. The observed differential number flux f [s⁻¹ m⁻² str⁻¹ MeV⁻¹] was integrated over the observed energy and pitch angle range to obtain the total number flux $F[s^{-1} m^{-2}]$ for each bin. Then, each R profile, representing the collision rate, was multiplied by the corresponding total number flux F to calculate the ionization rate profile for that bin. The ionization rates from all bins were finally summed to obtain the total ionization rate $Q [s^{-1} m^{-3}]$ as a function of altitude. The time variation of electron density $N_{\rm e}$ [m⁻³] due to production and recombina-

$$\frac{\mathrm{d}N_{\mathrm{e}}}{\mathrm{d}t} = Q - \alpha N_{\mathrm{e}}^2 \tag{2}$$

where α [m³ s⁻¹] is an effective recombination rate proposed by Gledhill (1986). The altitude (h [km]) profile of the recombination is given by

$$\alpha = 4.30 \times 10^{-12} \exp(-2.42 \times 10^{-2} h) + 8.16 \times 10^{6} \exp(-0.524 h),$$

which is a statistical estimate derived from electron density measurements during auroral events. Although image data

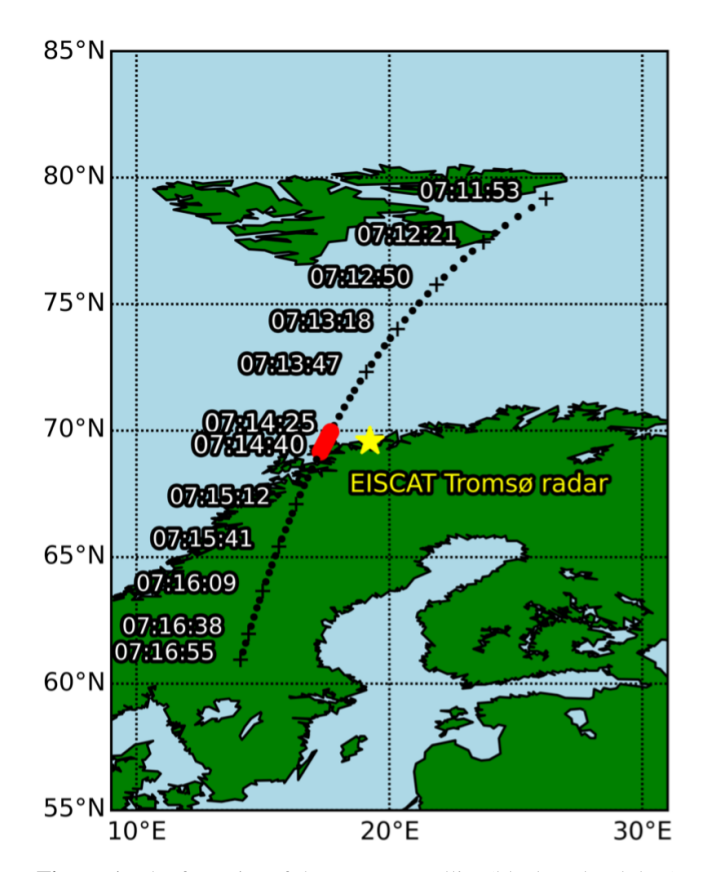


Figure 1. The footprint of the ELFIN satellite (black and red dots) and the location of the EISCAT Tromsø radar (yellow star). The red ones show the satellite footprint for 15 s when both were the closest during the event.

were not always available due to bad weather conditions, electron density enhancements were clearly identified in the auroral emission altitude region. Therefore, it is reasonable to apply this value of the recombination rate in the present analysis. The time derivative is important in high time resolution observations, which are able to follow the time variations. However, it is impossible to follow local time variations of the precipitating flux from the fast moving satellite, so the assumption that electron density is steady-state $(\frac{dN_e}{dt} = 0)$ is the most reasonable estimate that one is forced to use in this case. Thus, the electron density was calculated as $N_e = \sqrt{\frac{Q}{\alpha}}$. Then, the altitude profile of electron density was calculated both with and without consideration of the effect of the mirror force. The ratio of the density with the mirror force to that without the force at 80 km altitude is used as a metric of the mirror force effect, and we refer to this as the "density ratio". We showed the density ratios at an altitude of 80 km as representative values in this paper. Finally, a comparison was made between simulations and observations of the altitude profile of electron density during the 15 s when the footprint of the satellite and the radar were closest.

3 Results

3.1 Event on 16 December 2021

3.1.1 Event summery

There were four events in which the ELFIN satellite and the EISCAT Tromsø radar observed simultaneously, and the electron density increased under $100\,\mathrm{km}$ altitude. Especially in the event on 16 December 2021, at about 07:14 UT, the satellite footprint was the closest to the radar, and they were thought to be under simultaneous observation of an electron density enhancement in the atmosphere caused by EEP. In this event, the AE index was up to $300\,\mathrm{nT}$. The solar wind was quiet, with B_z at $-2\,\mathrm{nT}$ and SYM-H at $-16\,\mathrm{nT}$. Figure 1 shows the footprints of the ELFIN-A for about 5 min from around 07:12 UT and the location of the EISCAT Tromsø radar. The satellite traveled southward and was closest to the radar around 07:14:30 UT. The red dots show the satellite position during the 15 s for which we used the observation data in this study.

Figure 2a shows that the EISCAT Tromsø radar data observed electron density enhancement with a value more than $2 \times 10^{10} \,\mathrm{m}^{-3}$ for 10 min and that it had double peaks when the satellite was the closest to the radar, one was at 104.8 km altitude, and the other was at 94.7 km altitude in the electron density profile. It is assumed that an EEP observed by the satellite made the second peak. Figure 2b shows that the electrons have a wide range of pitch angles, from small angles up to 90°, and tend to be close to isotropic in the north of the radar, while most of the electrons had larger pitch angles than the loss cone angle at the southern range. It was also observed in Fig. 2c that most of the energetic electrons above 500 keV had large pitch angles, regardless of location. Figure 2d and e show that at the closest approach time, electrons with energy above 1000 keV were observed and that trapped electrons were the majority above 100 keV. Figure 2f shows the fraction of energy flux of precipitating, boundary, and trapped electrons separately among electrons with energy between 50 and 2500 keV. Note that the "boundary electrons" are defined as electrons observed in bins of the EPDE instrument in the satellite whose observation range includes the loss cone angle. Figure 2g is the density ratio at 80 km altitude, and Fig. 2h is the location of the ELFIN satellite. The time range in Fig. 2f and g is restricted between 07:13 and 07:16 because the number of electrons observed by the satellite at other times was not enough to be analyzed meaningfully. These three figures were compared in order to investigate trends in the density ratio. The density ratio decreased as the satellite went south; that is, the L value and the invariant latitude got smaller, and simultaneously, the ratio of trapped and boundary electrons became larger. For example, the density ratio was 0.8 at maximum when the trapped electrons occupied about half of the energy flux at the location with the L value of 10 and the invariant latitude of 72° . On the other hand, the value was 0.5 at minimum when the L value was five, and the invariant latitude was 63° . The trapped and boundary electrons were responsible for more than 75% of the total energy flux. The density ratio was especially 0.6 at the point where the footprint of the ELFIN satellite was the closest to the radar. In other words, we can say that the density ratio became smaller as the electrons with large pitch angles were more dominant in the distributions.

3.1.2 Data of the ELFIN satellite

Figure 3 shows the pitch angle and energy distribution of the electron number flux observed by the ELFIN satellite. The time range of Fig. 3b includes the time of closest approach of the satellite to the EISCAT Tromsø radar. As mentioned in the introduction, the effect of the mirror force is essential mainly for electrons with large pitch angles and with energy more than 100 keV. According to Fig. 3b, most electrons with energy less than 1000 keV had large pitch angles, though the pitch angle distribution of electrons with higher energy than 1000 keV did not show any apparent tendencies. Specifically, the number flux of 63 keV electrons, for example, was about $10^6 \,\mathrm{s^{-1}\,cm^{-2}\,str^{-1}\,MeV^{-1}}$ with a pitch angle larger than 70° while that was less than $10^5 \,\mathrm{s}^{-1} \,\mathrm{cm}^{-2} \,\mathrm{str}^{-1} \,\mathrm{MeV}^{-1}$ with a pitch angle less than 30°. The analysis for the entire observed energy range revealed that the electrons with pitch angles almost equal to or greater than the loss cone angle account for about 72 % of the total energy flux.

The distributions in Fig. 3a and c are the same as in Fig. 3b except for observation time, which has time ranges of 15 s before and after the time of Fig. 3b. These ELFIN satellite observations suggest that the trapped particles became slilghtly more dominant for lower-energy electrons (Sergeev et al., 2012). However, the electron density measurement by the EISCAT radar consistently shows the second peak of enhancement at around 95 km altitude (see Fig. 2a), which corresponds to tens-of-keV electrons at least according to the stopping height (Turunen et al., 2009). Therefore, although the satellite did not pass through just above the radar, it is reasonable to consider the comparison at the time of closest approach to be meaningful, since both instruments were likely observing precipitating electrons in a common energy range, and the resulting ionization profiles are comparable.

3.1.3 Simulation results and comparison with EISCAT observation data

Figure 4 shows three types of altitude profiles of the electron density. The black line is the EISCAT Tromsø radar data, while the red and blue lines are simulated electron density using the electron distribution shown in Fig. 3b as an initial condition with and without the mirror force effect, respectively. Each peak value at 87 km altitude of the red and blue lines in Fig. 4 is made by 63 keV electrons, which is the minimum value of observed energy. Because electrons with

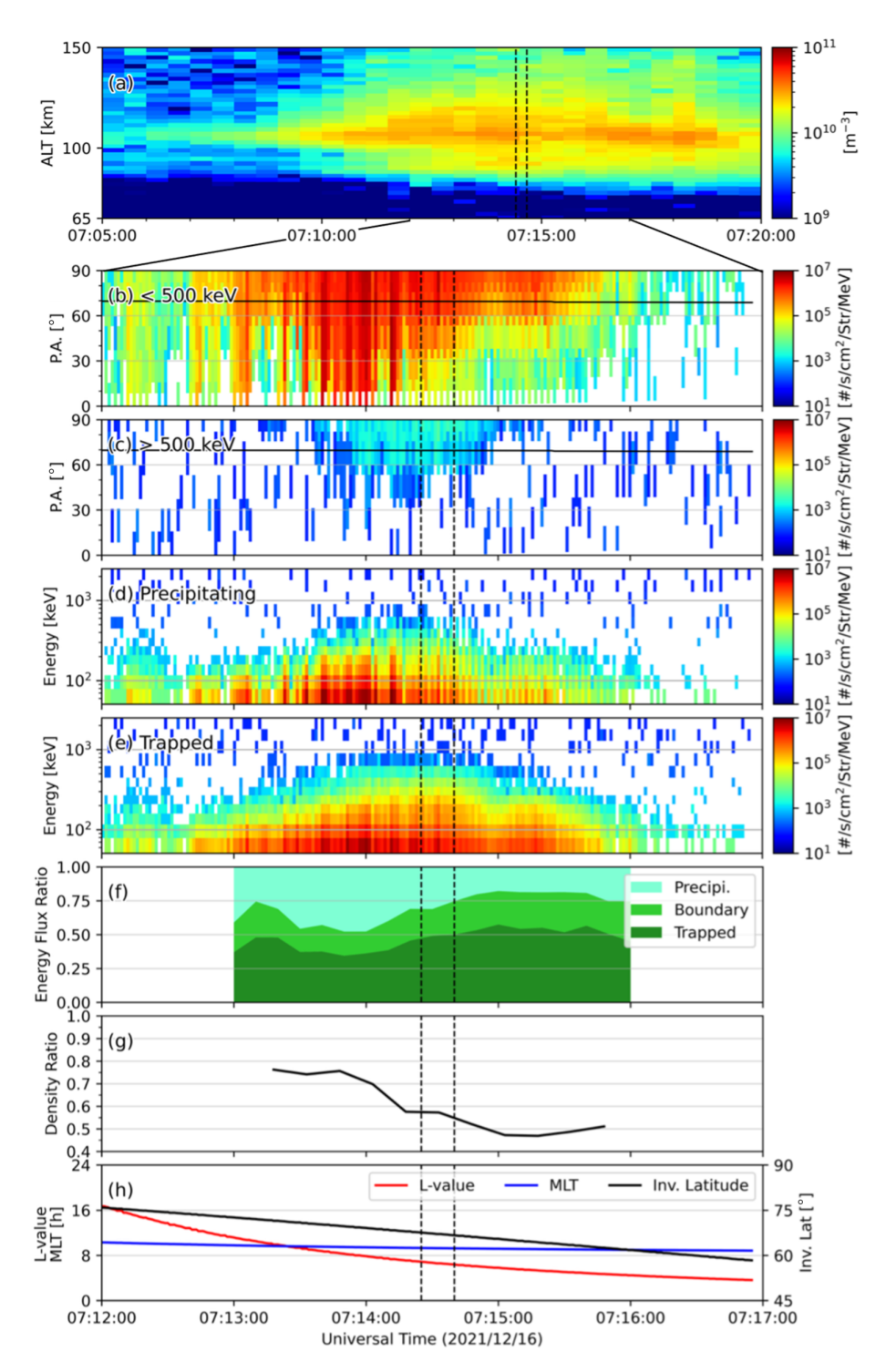


Figure 2. Simultaneous observation data of the EISCAT Tromsø radar (a) and the ELFIN satellite (b-f), and the simulation result (g). (a) Altitude profile of electron density observed by the EISCAT. (b) Average pitch angle distributions of the electron number flux below 500 keV were observed by the satellite. (c) Same as (b) but for that above 500 keV. (d) Average energy distributions of the electrons with the pitch angles less than the loss cone angle. (e) Same as (d) but for those more than the loss cone angle. (f) Fraction of the energy flux for precipitating, boundary, and trapped electrons. (g) The density ratio at 80 km altitude from the simulations with/without mirror force effect. (h) Information on the geomagnetic location of the satellite: L value, magnetic local time, and invariant latitude. Two vertical dashed lines show the 15 s time span of the closest approach of the satellite to the EISCAT, corresponding to the red dots in Fig. 1.

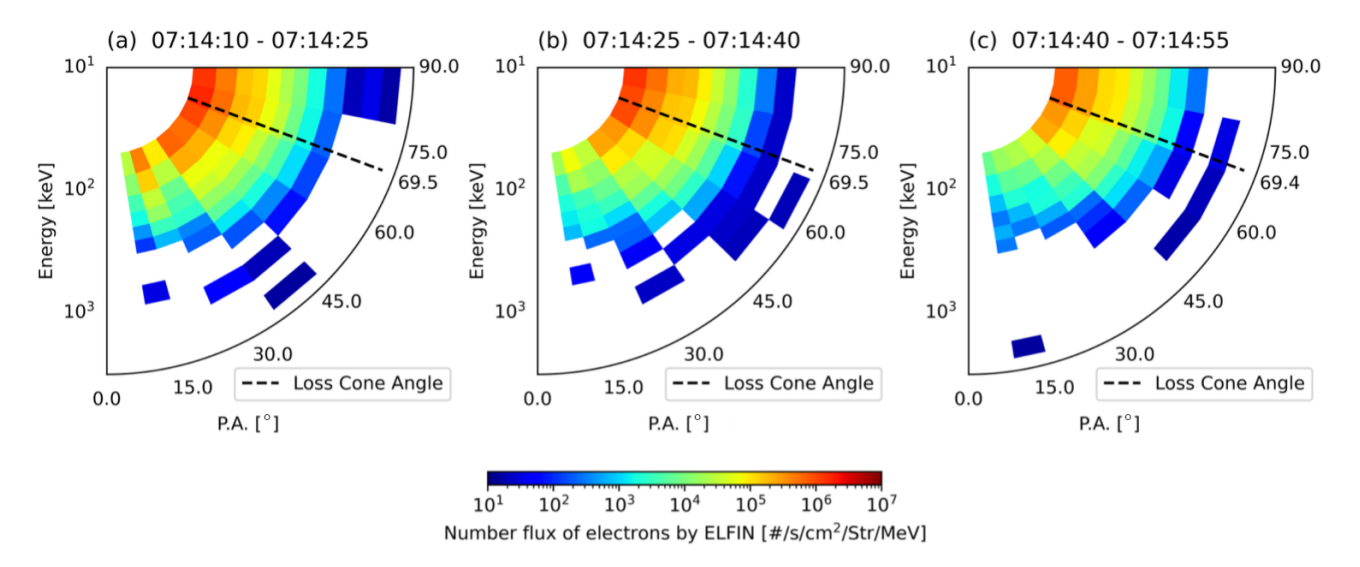


Figure 3. Pitch angle and energy distribution of the electron number flux observed by the ELFIN satellite, averaged during 15 s before (a), at the time (b), and after (c) the closest access of the satellite to the EISCAT Tromsø radar. Dashed lines indicate the loss cone angle.

energy less than 63 keV, out of observation, must have contributed to the atmospheric electron density above 87 km altitude, we compared the simulation results to the radar data at altitudes below 85 km (see Zou et al., 2024). The density ratio between the simulations with and without the mirror force effect is 0.6 at 80 km altitude, and the value does not change significantly in the altitude range below 85 km. The altitude profile of electron density observed by the EISCAT radar at the same time is generally smaller than the values obtained from the two simulation results. The density ratio between the "with simulation" ("without simulation") and the EIS-CAT observation at 80 km is 1.7 (2.9), respectively. Hence, this result suggests that it might be important to consider the reduction in ionization due to the mirror force effect when studying ionization processes caused by EEP at altitudes below 85 km.

3.2 The results of the other events and their characteristics

We investigated four events, including the one described in Sect. 3. Table 1 lists the date, time, and the density ratio at 80 km altitude. The table also shows the energy flux percentage of trapped electrons, including boundary electrons (Tra. E-flux), observed by the ELFIN satellite. We calculated these values using the data of the time when the satellite was closest approach to the EISCAT Tromsø radar at the magnetic latitude of 66° .

Figure 5 shows a comparison between the EISCAT radar observations and the simulation results for all four events. The event on 16 December 2021 (the most right panel), showed that the EISCAT radar was able to derive more accurate altitude profile of electron density. For three of the events, the observed electron density agrees more closely

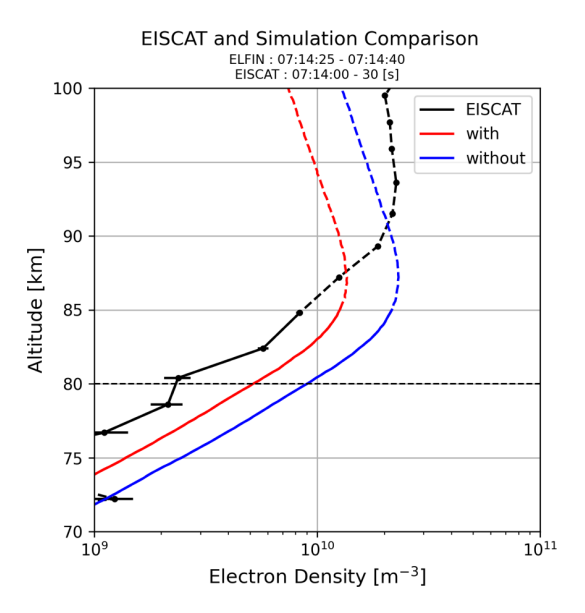


Figure 4. Altitude profile of electron density. Simulation results, with/without the mirror force effect, are shown by the red/blue lines, respectively. The black line shows the EISCAT Tromsø radar observation. Note that it is inappropriate to compare simulation results with the observed data above 85 km altitude because there must be an electron density enhancement due to lower energy electrons than observed by the ELFIN satellite.

with the simulation results with the mirror force than with those without the force, except for the event on 7 January. These results support taking the mirror force into account in calculations of electron density enhancement due to precipitating energetic electrons. On the other hand, the EISCAT radar did not observe a clear enhancement in electron den-

Table 1. Summary of conjunction events between the ELFIN satellite and EISCAT Tromsø radar.

Date (yyyy/mm/dd)	UT	Density ratio	Tra. E-flux
2020/12/09	21:31	0.80	35 %
2021/01/07	19:52	0.66	93 %
2021/10/05	20:20	0.59	61 %
2021/12/16	07:14	0.57	72 %

sity at low altitude on 5 October 2021, as would be expected based on the conjugate simulation result.

The density ratios ranged from 0.57 to 0.80. When the value was the smallest (0.57) on 16 December 2021, trapped or boundary electrons accounted for 72 % of the total energy flux. When the ratio increased to 0.80 on 9 December 2020, the energy flux carried by trapped or boundary electrons decreased to 35 % of the total, indicating a significant increase in the energy flux of electrons within the loss cone. Therefore, it was found that, as mentioned in Katoh et al. (2023), electrons with large pitch angles make a difference due to the mirror force, reducing the electron density in the atmosphere resulting from the actual distribution by approximately half (see Fig. 2) compared to the traditional method, which ignored the mirror force.

4 Discussion

To compare the overall altitude profile of electron density, the simulation results and observational data showed good agreement for the 16 December 2021 event (see Sect. 3.2 and Fig. 5), but not clearly for the other events. One of the reason for unclear comparison results in Fig. 5 is assumed to be the low signal-to-noise ratio of the electron density profile observed by the EISCAT Tromsø radar. It is known that the signal-to-noise ratio becomes significantly low when the electron density is less than $10^{10} \, \mathrm{m}^{-3}$, which has prevented accurate observation and comparison at an altitude of $80 \, \mathrm{km}$.

Another reason is mainly due to the spatial distance between the ELFIN satellite and the EISCAT Tromsø radar, but more accurate simulations are needed to compare its results to observational data, such as the introduction of secondary electrons. In detail, Fig. 4 also shows that the observed electron density was slightly lower than that calculated by the numerical simulation including the mirror force. This difference is most likely due to electrons scattered by whistlermode waves (e.g., Zhang et al., 2023), as the event is characterized by intense bursty precipitations. In that case, the electron flux is expected to vary on time scales of seconds, but the satellite could not capture it within a limited latitude range conjugated to the radar.

Additionally, the close timing of the observations does not necessarily indicate that the satellite and the radar observed the same precipitation event. As shown in Fig. 6, during the

closest 15 s, the satellite footprint (red line) includes both discrete aurora and diffuse aurora, whereas the radar only observed the diffuse aurora region. Furthermore, as seen in Fig. 3, slight changes in latitude caused some variations in pitch angle and energy distributions. Therefore, small differences in the observed precipitation event may have led to discrepancies between the simulation and the observation results.

Moreover, the difference in integration time between the two instruments (ELFIN: 15 s; EISCAT: 30 s) makes it even less certain that they observed the same precipitation. Neverthless, it is by chance that the conjunction event occurred during an EEP event. Since events where satellites and radars can closely observe the same region are difficult to capture, it is important to utilize other incoherent scatter radars, such as the PFISR (Poker Flat Incoherent Scatter Radar) in Alaska, to find additional events and validate the mirror force effect.

The ionization profile during EEP is affected not only by pitch angle distribution but also by energy distribution. Katoh et al. (2023) found that the difference due to the consideration of the mirror force becomes more evident for electrons with higher energy. Additionally, the ratio of energy flux of trapped electrons always increases with energy when EEP occurs due to the whistler-mode waves (e.g., Tsai et al., 2024). Both results support the idea that higher energy electrons are more likely to be affected by the mirror force, which reduces the electron density in the atmosphere. On the other hand, it is known that the ratio sometimes remains constant for the 50–1000 keV range during intense precipitations by high-intensity waves (Zhang et al., 2022) and that the ratio increases if precipitation is driven by EMIC waves (Capannolo et al., 2023). These studies suggest that the significance of the effect of the mirror force depends on wave strength or type, but we only found whistler-mode wave events in our conjugated observation. Therefore, it is necessary to statistically investigate the force's contribution to the electron density in the atmosphere with a focus on the type of wave.

In this study, we also examined the latitudinal distribution of the density ratio for only one event (see Fig. 2g). We found that the difference due to the mirror force depends on latitude and that the ratio is more likely to be smaller as latitude decreases, even while electrons seemed to be precipitating from the radiation belt. This is because the distribution of electrons depends on latitude. Specifically, this is because the percentage of trapped electrons was more significant at lower latitudes. It is also statistically consistent with Qin's finding that the smaller the L value, the larger the ratio of energy flux of trapped electrons. However, the effects of the mirror force, i.e., the variations in density ratios due to distribution changes in both the energy and pitch angle, are not yet fully understood, so more ELFIN satellite observation events should be used to examine the latitudinal distribution of the ratio.

Finally, this study focused on the magnetic mirror force and included its effects in the simulation to see how it

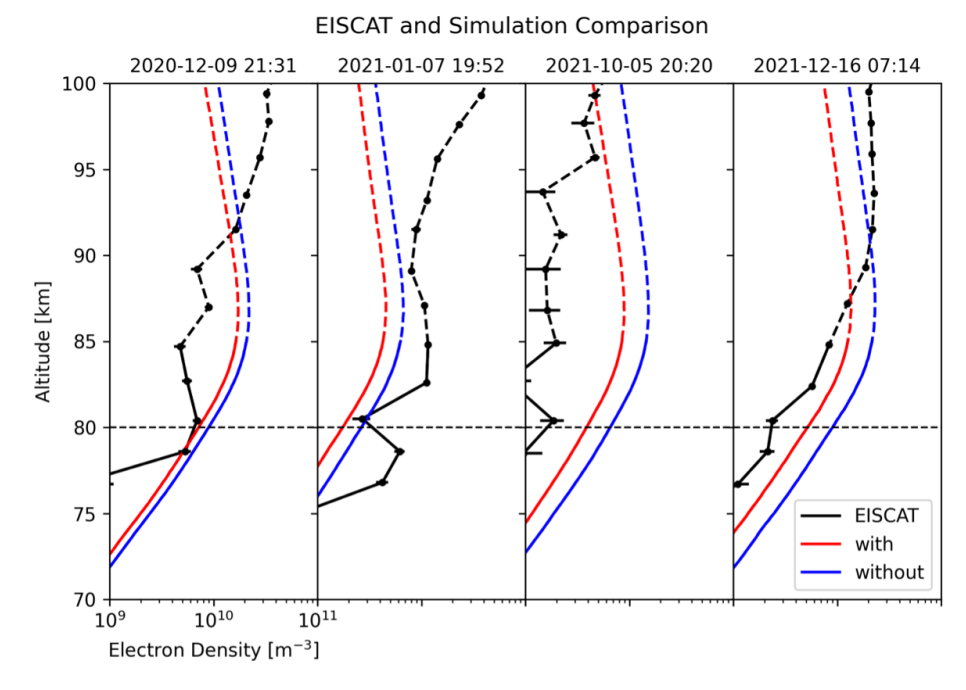


Figure 5. Electron density comparison between the EISCAT radar observation and simulations. The black lines are the observation results, and the red and blue lines indicate the simulation results with and without the mirror force, respectively.

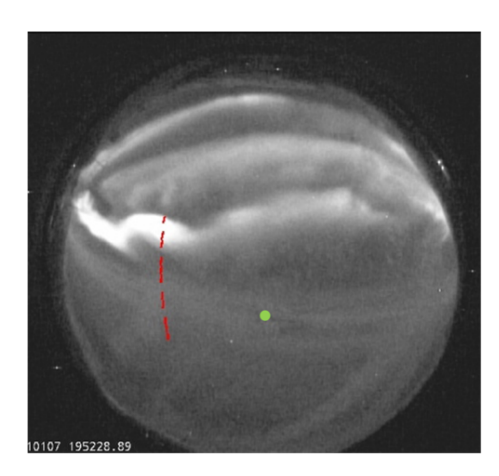


Figure 6. Optical data collected by at Tromsø on 7 January 2021. The red dashed line is the satellite footprint, and the green dot indicates the radar beam point.

changes the electron density enhancement in the atmosphere. It was mentioned in Katoh et al. (2023) that some electrons move back away from the atmosphere, i.e., go up again. However, even though the ELFIN satellite observed the flux of upgoing electrons, a comparison between the observational data and the simulation results has yet to be made. In the future, it can be verified whether the upgoing electrons observed would be consistent with the simulation results by improving the simulation code so that the energy and pitch angle distributions of the reflected electrons can be calculated.

5 Conclusion

This study aims to evaluate the effect of the mirror force on precipitating electrons and, consequently, atmospheric electron density by focusing on the pitch angle of electrons. We used ELFIN satellite data and a simulation developed by Katoh et al. (2023). We found that the electron density due to EEP can be about 40 % smaller when the effect of the mirror force is considered than when it ignored the effect as in previous studies (e.g., Murase et al., 2023). The simulation results were compared with simultaneous data from the EIS-CAT Tromsø radar. For an event where the altitude profile of electron density was accurately determined from the EIS-CAT radar on 16 December 2021, the simulated electron density profile, including the mirror force effect, is closer to the actual density profile from EISCAT than when ignoring the effect. Furthermore, although this is not a conjunction event between the ELFIN satellite and the radar, some pitch angle distribution made the ratio reach 50 % at maximum. In other words, these results suggest the importance of considering the pitch angle distribution of electrons and the effect of EEP on the simulation of electron density enhancement in the atmosphere, or the result would differ by about 50 %. Additionally, in order to accurately estimate the effects of atmospheric ionisation, it is desirable for electron instruments with Low Earth Orbit (LEO) satellites to observe pitch angle distributions with high resolution, which can distinguish between trapped and precipitating particles.

Code availability. The simulation code used in this study was developed by Katoh et al. (2023) and has been utilized in an advanced project. The code is not publicly available at this time because the project is still in progress.

Data availability. ELFIN data can be publicly available from https://data.elfin.ucla.edu (last access: 20 October 2025). Level 1 data are provided in CDF format and can be processed using SPEDAS (https://spedas.org/blog/, last access: 20 October 2025) or pySPEDAS (https://github.com/spedas/pyspedas, last access: 20 October 2025, Grimes et al., 2022) subroutines (see Angelopoulos et al., 2019, 2020). Raw EISCAT data used in this study are available at https://portal.eiscat.se/schedule (last access: 20 October 2025), and the GUISDAP software used to analyze the EISCAT raw data is available at https://eiscat.se/scientist/user-documentation/guisdap/ (last access: 20 October 2025).

Author contributions. YO designed this study. YK instructed TT on the use of simulation he developed. AA, VA, and XZ collected and proceeded the data observed by the ELFIN satellites. YO, YK, AK, YT, and MF supervised the work. MF and TT analysed the data. TT made the figures and drafted the manuscript. All authors discussed the results and approaved the manuscript.

Competing interests. The contact author has declared that none of the authors has any competing interests.

Disclaimer. Publisher's note: Copernicus Publications remains neutral with regard to jurisdictional claims made in the text, published maps, institutional affiliations, or any other geographical representation in this paper. While Copernicus Publications makes every effort to include appropriate place names, the final responsibility lies with the authors. Views expressed in the text are those of the authors and do not necessarily reflect the views of the publisher.

Acknowledgements. EISCAT is an international association supported by research organisations in China (CRIRP), Finland (SA), Japan (NIPR and ISEE), Norway (NFR), Sweden (VR), and the United Kingdom (UKRI). The authors acknowledge all members of the ELFIN teams for providing data.

Financial support. This research was supported by the Grants-in-Aid for Scientific Research (grant nos. 20K04052, 20KK0313, and 23H05429) by the Ministry of Education, Science, Sports and Culture, Japan. This research was also supported by the JSPS Fellowship Program "Invitational Fellowships for Research". This paper is financially supported by the NIPR Paper Publication Support Program.

Review statement. This paper was edited by Minna Palmroth and reviewed by two anonymous referees.

References

Alken, P., Thébault, E., Beggan, C. D., Amit, H., Aubert, J., Baerenzung, J., Bondar, T. N., Brown, W. J., Califf, S., Chambodut, A., Chulliat, A., Cox, G. A., Finlay, C. C., Fournier, A., Gillet, N., Grayver, A., Hammer, M. D., Holschneider, M., Huder, L., Hulot, G., Jager, T., Kloss, C., Korte, M., Kuang, W., Kuvshinov, A., Langlais, B., Léger, J.-M., Lesur, V., Livermore, P. W., Lowes, F. J., Macmillan, S., Magnes, W., Mandea, M., Marsal, S., Matzka, J., Metman, M. C., Minami, T., Morschhauser, A., Mound, J. E., Nair, M., Nakano, S., Olsen, N., Pavón-Carrasco, F. J., Petrov, V. G., Ropp, G., Rother, M., Sabaka, T. J., Sanchez, S., Saturnino, D., Schnepf, N. R., Shen, X., Stolle, C., Tangborn, A., Tøffner-Clausen, L., Toh, H., Torta, J. M., Varner, J., Vervelidou, F., Vigneron, P., Wardinski, I., Wicht, J., Woods, A., Yang, Y., Zeren Z., and Zhou, B.: International Geomagnetic Reference Field: the thirteenth generation, Earth Planets Space, 73, 49, https://doi.org/10.1186/s40623-020-01288-x, 2021.

Angelopoulos, V., Cruce, P., Drozdov, A., Grimes, E. W., Hatzigeorgiu, N., King, D. A., Larson, D., Lewis, J. W., McTiernan, J. M., Roberts, D. A., Russell, C. L., Hori, T., Kasahara, Y., Kumamoto, A., Matsuoka, A., Miyashita, Y., Miyoshi, Y., Shinohara, I., Teramoto, M., Faden, J. B., Halford, A. J., McCarthy, M., Millan, R. M., Sample, J. G., Smith, D. M., Woodger, L. A., Masson, A., Narock, A. A., Asamura, K., Chang, T. F., Chiang, C.-Y., Kazama, Y., Keika, K., Matsuda, S., Segawa, T., Seki, K., Shoji, M., Tam, S. W. Y., Umemura, N., Wang, B.-J., Wang, S.-Y., Redmon, R., Rodriguez, J. V., Singer, H. J., Vandegriff, J., Abe, S., Nose, M., Shinbori, A., Tanaka, Y.-M., UeNo, S., Andersson, L., Dunn, P., Fowler, C., Halekas, J. S., Hara, T., Harada, Y., Lee, C. O., Lillis, R., Mitchell, D. L., Argall, M. R., Bromund, K., Burch, J. L., Cohen, I. J., Galloy, M., Giles, B., Jaynes, A. N., Le Contel, O., Oka, M., Phan, T. D., Walsh, B. M., Westlake, J., Wilder, F. D., Bale, S. D., Livi, R., Pulupa, M., Whittlesey, P., De-Wolfe, A., Harter, B., Lucas, E., Auster, U., Bonnell, J. W., Cully, C. M., Donovan, E., Ergun, R. E., Frey, H. U., Jackel, B., Keiling, A., Korth, H., McFadden, J. P., Nishimura, Y., Plaschke, F., Robert, P., Turner, D. L., Weygand, J. M., Candey, R. M., Johnson, R. C., Kovalick, T., Liu, M. H., McGuire, R. E., Breneman, A., Kersten, K., and Schroeder, P.: The Space Physics Environment Data Analysis System (SPEDAS), Space Sci. Rev., 215, 9, https://doi.org/10.1007/s11214-018-0576-4, 2019.

Angelopoulos, V., Tsai, E., Bingley, L., Shaffer, C., Turner, D. L., Runov, A., Li, W., Liu, J., Artemyev, A. V., Zhang, X.-J., Strangeway, R. J., Wirz, R. E., Shprits, Y. Y., Sergeev, V. A., Caron, R. P., Chung, M., Cruce, P., Greer, W., Grimes, E., Hector, K., Lawson, M. J., Leneman, D., Masongsong, E. V., Russell, C. L., Wilkins, C., Hinkley, D., Blake, J. B., Adair, N., Allen, M., Anderson, M., Arreola-Zamora, M., Artinger, J., Asher, J., Branchevsky, D., Capitelli, M. R., Castro, R., Chao, G., Chung, N., Cliffe, M., Colton, K., Costello, C., Depe, D., Domae, B. W., Eldin, S., Fitzgibbon, L., Flemming, A., Fox, I., Frederick, D. M., Gilbert, A., Gildemeister, A., Gonzalez, A., Hesford, B., Jha, S., Kang, N., King, J., Krieger, R., Lian, K., Mao, J., McKinney, E., Miller, J. P., Norris, A., Nuesca, M., Palla, A., Park, E. S. Y., Pedersen, C. E., Qu, Z., Rozario, R., Rye, E., Seaton, R., Subramanian, A., Sundin, S. R., Tan, A., Turner, W., Villegas, A. J., Wasden, M., Wing, G., Wong, C., Xie, E., Yamamoto, S., Yap, R., Zarifian, A., and Zhang, G. Y.: The ELFIN Mission, Space

- Sci. Rev., 216, 103, https://doi.org/10.1007/s11214-020-00721-7-2020
- Capannolo, L., Li, W., Ma, Q., Qin, M., Shen, X.-C., Angelopoulos, V., Artemyev, A., Zhang, X.-J., and Hanzelka, M.: Electron Precipitation Observed by ELFIN Using Proton Precipitation as a Proxy for Electromagnetic Ion Cyclotron (EMIC) Waves, Geophysical Research Letters, 50, e2023GL103519, https://doi.org/10.1029/2023GL103519, 2023.
- Emmert, J. T., Jones Jr., M., Siskind, D. E., Drob, D. P., Picone, J. M., Stevens, M. H., Bailey, S. M., Bender, S., Bernath, P. F., Funke, B., Hervig, M. E., and Pérot, K.: NRLMSIS 2.1: An Empirical Model of Nitric Oxide Incorporated Into MSIS, Journal of Geophysical Research: Space Physics, 127, e2022JA030896, https://doi.org/10.1029/2022JA030896, 2022.
- Folkestad, K., Hagfors, T., and Westerlund, S.: EISCAT: An updated description of technical characteristics and operational capabilities, Radio Science, 18, 867–879, https://doi.org/10.1029/RS018i006p00867, 1983.
- Gledhill, J. A.: The effective recombination coefficient of electrons in the ionosphere between 50 and 150 km, Radio Science, 21, 399–408, https://doi.org/10.1029/RS021i003p00399, 1986.
- Grimes, E. W., Harter, B., Hatzigeorgiu, N., Drozdov, A., Lewis, J. W., Angelopoulos, V., Cao, X., Chu, X., Hori, T., Matsuda, S., Jun, C.-W., Nakamura, S., Kitahara, M., Segawa, T., Miyoshi, Y., and Le Contel, O.: The Space Physics Environ-ment Data Analysis System in Python, Front. Astron. Space Sci.,9, 1020815, https://doi.org/10.3389/fspas.2022.1020815, 2022.
- Katoh, Y., Rosendahl, P. S., Ogawa, Y., Hiraki, Y., and Tadokoro, H.: Effect of the mirror force on the collision rate due to energetic electron precipitation: Monte Carlo simulations, Earth Planets Space, 75, 117, https://doi.org/10.1186/s40623-023-01871-y, 2023.
- Lehtinen, M. and Huuskonen, A.: General incoherent scatter analysis and GUISDAP, J. Atmos. Terr. Phys., 58, 435–452, https://doi.org/10.1016/0021-9169(95)00047-X, 1996.
- Lehtinen, N. G., Bell, T. F., and Inan, U. S.: Monte Carlo simulation of runaway MeV electron breakdown with application to red sprites and terrestrial gamma ray flashes, Journal of Geophysical Research: Space Physics, 104, 24699–24712, https://doi.org/10.1029/1999JA900335, 1999.
- Lucas, G.: pymsis, Zenodo [code], https://doi.org/10.5281/zenodo.5348502, 2022.
- Miyoshi, Y., Saito, S., Kurita, S., Asamura, K., Hosokawa, K., Sakanoi, T., Mitani, T., Ogawa, Y., Oyama, S., Tsuchiya, F., Jones, S. L., Jaynes, A. N., and Blake, J. B.: Relativistic Electron Microbursts as High-Energy Tail of Pulsating Aurora Electrons, Geophysical Research Letters, 47, e2020GL090360, https://doi.org/10.1029/2020GL090360, 2020.
- Miyoshi, Y., Hosokawa, K., Kurita, S., Oyama, S.-I., Ogawa, Y., Saito, S., Shinohara, I., Kero, A., Turunen, E., Verronen, P. T., Kasahara, S., Yokota, S., Mitani, T., Takashima, T., Higashio, N., Kasahara, Y., Matsuda, S., Tsuchiya, F., Kumamoto, A., Matsuoka, A., Hori, T., Keika, K., Shoji, M., Teramoto, M., Imajo, S., Jun, C., and Nakamura, S.: Penetration of MeV electrons into the mesosphere accompanying pulsating aurorae, Sci. Rep., 11, 13724, https://doi.org/10.1038/s41598-021-92611-3, 2021.
- Murase, K., Kataoka, R., Nishiyama, T., Nishimura, K., Hashimoto, T., Tanaka, Y., Kadokura, A., Tomikawa, Y., Tsutsumi, M., Ogawa, Y., Uchida, H. A., Sato, K., Kasahara, S., Mitani, T.,

- Yokota, S., Hori, T., Keika, K., Takashima, T., Kasahara, Y., Matsuda, S., Shoji, S., Matsuoka, A., Shinohara, I., Miyoshi, Y., Sato, T., Ebihara, Y., and Tanaka, T.: Mesospheric ionization during substorm growth phase, J. Space Weather Space Clim., 12, 18, https://doi.org/10.1051/swsc/2022012, 2022.
- Murase, K., Kataoka, R., Nishiyama, T., Sato, K., Tsutsumi, M., Tanaka, Y., Ogawa, Y., and Sato, T.: Atmospheric Ionizations by Solar X-Rays, Solar Protons, and Radiation Belt Electrons in September 2017 Space Weather Event, Space Weather, 21, e2023SW003651, https://doi.org/10.1029/2023SW003651, 2023.
- Nesse Tyssøy, H., Sinnhuber, M., Asikainen, T., Bender, S., Clilverd, M. A., Funke, B., van de Kamp, M., Pettit, J. M., Randall, C. E., Reddmann, T., Rodger, C. J., Rozanov, E., Smith-Johnsen, C., Sukhodolov, T., Verronen, P. T., Wissing, J. M., and Yakovchuk, O.: HEPPA III Intercomparison Experiment on Electron Precipitation Impacts: 1. Estimated Ionization Rates During a Geomagnetic Active Period in April 2010, Journal of Geophysical Research-Space Physics, 127, e2021JA029128, https://doi.org/10.1029/2021JA029128, 2022.
- Oyama, S., Kero, A., Rodger, C. J., Clilverd, M. A., Miyoshi, Y., Partamies, N., Turunen, E., Raita, T., Verronen, P. T., and Saito, S.: Energetic electron precipitation and auroral morphology at the substorm recovery phase, Journal of Geophysical Research-Space Physics, 122, 6508–6527, https://doi.org/10.1002/2016JA023484, 2017.
- Ozaki, M., Shiokawa, K., Kataoka, R., Mlynczak, M., Paxton, L., Connors, M., Yagitani, S., Hashimoto, S., Otsuka, Y., Nakahira S., and Mann, I.: Localized mesospheric ozone destruction corresponding to isolated proton aurora coming from Earth's radiation belt, Sci. Rep., 12, 16300, https://doi.org/10.1038/s41598-022-20548-2, 2022.
- Rees, M. H.: Auroral ionization and excitation by incident energetic electrons, Planetary and Space Science, 11, 1209–1218, https://doi.org/10.1016/0032-0633(63)90252-6, 1963.
- Sergeev, V., Nishimura, Y., Kubyshkina, M., Angelopoulos, V., Nakamura, R., and Singer, H.: Magnetospheric location of the equatorward prebreakup arc, J. Geophys. Res., 117, A01212, https://doi.org/10.1029/2011JA017154, 2012.
- Solomon, S. C.: auroral electron transport using the Monte Carlo Method, Geophysical Research Letters, 20, 185–188, https://doi.org/10.1029/93GL00081, 1993.
- Solomon, S. C.: Auroral particle transport using Monte Carlo and hybrid methods, Journal of Geophysical Research-Space Physics, 106, 107–116, https://doi.org/10.1029/2000JA002011, 2001.
- Tsai, E., Artemyev, A., Anglelopoulos, V., and Zhang, X.-J.: Investing Whistler-Mode Intensity Along Field Lines Using Electron Precipitation Measurements, Journal of Geophysical Research-Space Physics, 128, e2023JA031578, https://doi.org/10.1029/2023JA031578, 2023.
- Tsai, E., Artemyev, A., Ma, Q., Mourenas, D., Agapitov, O., Zhang, X.-J., and Angelopoulos, V.: Key Factors Determining Nightside Energetic Electron Losses Driven by Whistler-Mode Waves, Journal of Geophysical Research-Space Physics, 129, e2023JA032351, https://doi.org/10.1029/2023JA032351, 2024.
- Turunen, E., Verronen, P. T., Seppälä, A., Rodger, C. J., Clilverd, M. A., Tamminen, J., Enell, C.-F., and Ulich, T.: Impact of different energies of precipitating particles on NOx

- generation in the middle and upper atmosphere during geomagnetic storms, J. Atmos. Sol. Terr. Phys., 71, 1176–1189, https://doi.org/10.1016/j.jastp.2008.07.005, 2009.
- Turunen, E., Kero, A., Verronen, P. T., Miyoshi, Y., Oyama, S.-I., and Saito, S.: Mesospheric ozone destruction by high-energy electron precipitation associated with pulsating aurora, Journal of Geophysical Research-Atmospheres, 121, 11852–11861, https://doi.org/10.1002/2016JD025015, 2016.
- Xu, W., Marshall, R. A., Tyssøy, H. N., and Fang, X.: A Generalized Method for Calculating Atmospheric Ionization by Energetic Electron Precipitation, Journal of Geophysical Research-Space Physics, 125, e2020JA028482, https://doi.org/10.1029/2020JA028482, 2020.
- Zhang, X.-J., Angelopoulos, V., Mourenas, D., Artemyev, A., Tsai, E., and Wilkins, C.: Characteristics of Electron Microburst Precipitation Based on High-Resolution ELFIN Measurements, Journal of Geophysical Research-Space Physics, 127, e2022JA030509, https://doi.org/10.1029/2022JA030509, 2022.

- Zhang, X.-J., Angelopoulos, V., Artemyev, A., Mourenas, D., Agapitov, O., Tsai, E., and Wilkins, C.: Temporal Scales of Electron Precipitation Driven by Whistler-Mode Waves, Journal of Geophysical Research-Space Physics, 128, e2022JA031087, https://doi.org/10.1029/2022JA031087, 2023.
- Zou, Y., Zhang X.-J., Artemyev, A., Shen, Y., and Angelopoulos, V.: The Key Role of Magnetic Curvature Scattering in Energetic Electron Precipitation During Substorm, Journal of Geophysical Research Letters, 51, e2024GL109227, https://doi.org/10.1029/2024GL109227, 2024.